ELSEVIER

A practical method to detect and correct for lens distortion in the TEM

Gian Carlo Capitani[a],*, Peter Oleynikov[b], Sven Hovmöller[b], Marcello Mellini[c]

[a]*Dipartimento Geomineralogico, Bari University, Via Orabona 4, I-70125 Bari, Italy*
[b]*Department of Structural Chemistry, Stockholm University, SE-10691 Stockholm, Sweden*
[c]*Dipartimento di Scienze della Terra, Siena University, Via Laterina 8, I-53100 Siena, Italy*

Abstract

A practical, offline method for experimental detection and correction for projector lens distortion in the transmission electron microscope (TEM) operating in high-resolution (HR) and selected area electron diffraction (SAED) modes is described. Typical TEM works show that, in the simplest case, the distortion transforms on the recording device, which would be a circle into an ellipse. The first goal of the procedure described here is to determine the elongation and orientation of the ellipse. The second goal is to correct for the distortion using an ordinary graphic program. The same experimental data set may also be used to determine the actual microscope magnification and the rotation between SAED patterns and HR images.

The procedure may be helpful in several quantitative applications of electron diffraction and HR imaging, for instance while performing accurate lattice parameter determination, or while determining possible metrical deviations (cell edges and angles) from a given symmetry.

1. Introduction

The recent improvement of modern microscopes and the development of image processing techniques have made electron crystallography an alternative or complementary method to X-ray diffraction for solving crystal structures. Whenever the crystal size is too small for single crystal X-ray diffraction and X-ray powder diffraction is unsuited for structural analysis, electron crystallography may be the answer to the problem. Successful crystal structure determinations are

---

*Corresponding author. Tel.: +390805442608;
fax: +390805442591.

E-mail address: g.capitani@geomin.uniba.it
(G.C. Capitani).

reported for membrane proteins [1–3], organic molecules [4–6], and inorganic compounds [7–9]. Further advantages of electron crystallography versus X-ray diffraction appear evident when dealing with modulated structures, where one immediately gains information about the modulation wave-vector [10,11].

Many different theories have been developed, based either on kinematical or dynamical scattering, or exploiting either direct or reciprocal space or both. A number of program packages founded on these theories nowadays allow a painless approach to electron crystallography [11–16]. Whatever the preferred technique, in order to trust electron microscopy data one needs not only specific experimental conditions but also accurate data measurements. The microscope must be perfectly aligned and the aberrations well corrected for. Distortion is a kind of spherical aberration which mainly affects the projector lenses. In the presence of distortion, rays from each point of the object (the magnified intermediate image formed by the objective lens) reunite at corresponding points in the image plane, but the magnification varies throughout the plane. Depending on the way in which this variation occurs, one classically distinguishes pincushion, barrel, and spiral distortion (Fig. 1). The effects of all three kinds of distortion are most noticeable at low magnifications since, in this situation, a large area of the intermediate image formed by the objective lens is accepted by the projector lens(es). Barrel and pincushion distortion could be negligible even in old microscopes with large (say 3.3 mm) spherical aberration constant (C_s) and low (say

100 kV) accelerating voltage [17]. Spiral distortion is related to the rotation of the image that takes place in the magnetic electron lenses. Modern designs of magnetic electron lenses allow spiral distortion to be almost completely removed [18,19], or at least maintained below 1% if one has to work with beams subtending very large diffracting angles [20]. Our experience in dealing with HR imaging and SA diffraction reveals that the most relevant image affecting distortion can be approximated to be elliptical (Fig. 1e). In this paper, we present a practical method for the detection and correction of lens magnification distortion in the transmission electron microscope when operating in diffraction and high-resolution modes and the elliptical distortion is the most relevant aberration.

2. Experimental

Images and electron diffraction patterns were taken on a JEOL JEM2010 electron microscope (University of Siena), operating at 200 kV and equipped with URP (ultra-high resolution) pole-pieces ($C_s = 0.5$ mm), capable of 1.9 Å point-to-point resolution. The electron beam source was a monocrystalline LaB_6 emitter. Specimen alignment was achieved using a double tilt holder. Images were recorded on Fuji imaging plates (and then on conventional photographic films for comparison). Normal alignment procedures had been carefully followed before every TEM session. Therefore, we expect that the microscope was operating in quite standard HRTEM conditions, comparable to the
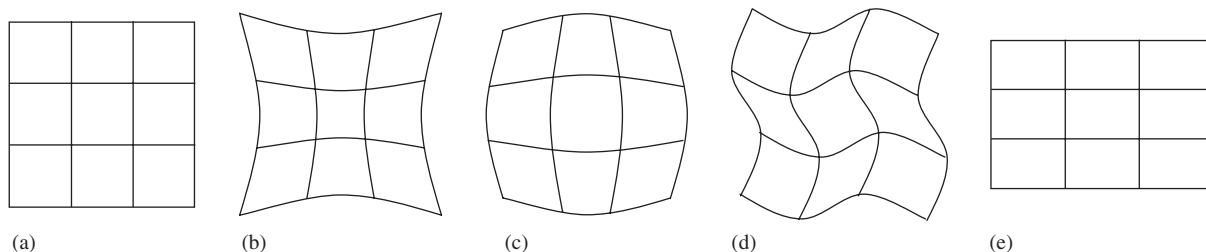

Fig. 1. (a) Undistorted image of the object; (b) pincushion distortion: magnification increases with distance from the axis and depends on the direction in which it is measured; (c) barrel distortion: magnification decreases with distance from the axis; (d) spiral distortion: a straight line is imaged as a sigmoidal shape; (e) elliptical distortion: the magnification is different in different radial directions.
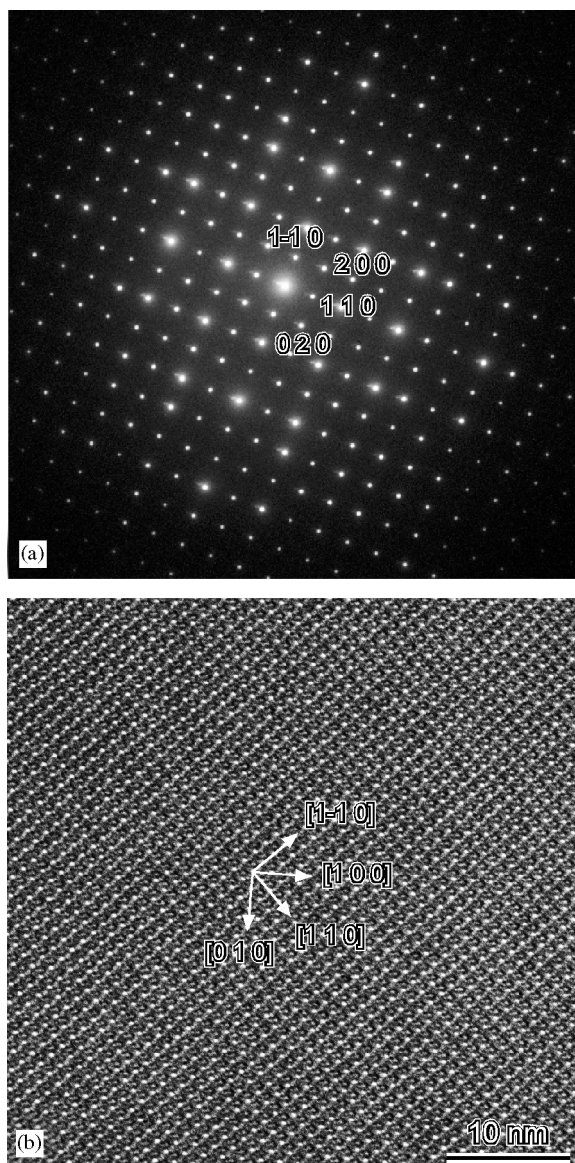
Fig. 2. (a) Selected area electron diffraction pattern of vesuvianite at 120 cm camera length. (b) HRTEM image of vesuvianite as seen down [0 0 1] at 600k × .

ones used in any other TEM laboratory, daily busy with acquisition of high-resolution images and as-accurate-as-possible electron diffraction work.

For the present study, a thin foil of a tetragonal crystal with its four-fold axis parallel to the

incident beam direction suits very well. We used here an ion-thinned vesuvianite crystal (with ideal formula $Ca_{19}Al_{11}Mg_2Si1_8O_{69}(OH)_9$ and unit cell dimensions $a = 15.639$ Å, $c = 13.092$ Å); in principle, any crystal with four-fold (or six-fold) symmetry along the observation direction and not subject to beam damage can be used. For reasons that will be clear in the following, it is useful to know the cell constants of the crystal from experiments other than TEM. A large vesuvianite crystal was broken and a fragment used to prepare the TEM mount. The remaining fragments were crushed and used for lattice constant refinement by least-squares fitting of X-ray powder diffraction peaks.

In keeping with Smith et al. [21], the microscope was properly aligned, and after selection of a well-ordered thin region, the sample was aligned with its four-fold axis parallel to the optical axis of the microscope. Selected area electron diffraction (SAED) patterns of the same area were taken with different camera lengths, among the most commonly used in daily practice, nominally 120, 150 and 200 cm. The microscope was then switched to imaging mode and the same areas were imaged at magnifications of 400, 600, 800k × and 1M × (Fig. 2).

3. Results

3.1. Image and diffraction measurements

For each diffraction pattern, the lengths of two sets of symmetry-related reciprocal lattice vectors were measured (the first formed by 100, 010, $\bar{1}00, 0\bar{1}0$; the second by 110, $1\bar{1}0, \bar{1}10, \bar{1}\bar{1}0$), along with the angle that they form with a reference direction (in the present case the horizontal x-axis). In the absence of distortion, all the four vectors in each set should be equally long, with the diagonal vectors related to the reciprocal lattice constants by $\sqrt{2}$. In the presence of elliptical lens distortion, only Friedel couples equate and each couple differs by a certain amount from the average value (Table 1). The precise amount of the deviation from the ideal conditions and the orientation of

Table 1
Orientations of the reciprocal vectors, with respect to the horizontal reference x-axis and normalized values (with respect to the average) of the g-vector modules, for different camera lengths (patterns collected on image plates)

| Camera length	120 cm		150 cm		200 cm	
	Angle (deg)	$g_{hkl}/\langle g_{hkl}\rangle$	Angle (deg)	$g_{hkl}/\langle g_{hkl}\rangle$	Angle (deg)	$g_{hkl}/\langle g_{hkl}\rangle$
020	−66.9	0.9979	−64.8	0.9980	−57.8	0.9955
110	−21.3	0.9925	−19.3	0.9915	−12.2	0.9917
200	24.0	1.0022	26.1	1.0025	33.3	1.0045
1–10	68.4	1.0074	70.5	1.0080	77.6	1.0083
0–20	113.1	0.9979	115.2	0.9980	122.2	0.9955
−1–10	158.7	0.9925	160.7	0.9915	167.8	0.9917
−200	204.0	1.0022	206.1	1.0025	213.3	1.0045
−110	248.4	1.0074	250.5	1.0080	257.6	1.0083

g_{h00} and g_{0h0} values divided by $2^{1/2}$.
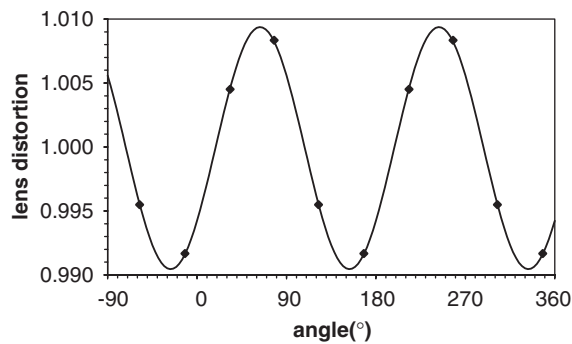
Fig. 3. Distortion in a diffraction pattern, given as ratios between observed and average interplanar spacings ($d_{hkl}/\langle d_{110}\rangle$) versus orientation to the reference horizontal x-axis for 200 cm camera length.

the ellipse can be deduced by plotting the measured values normalized to their average value versus the angles to the reference x-axis, and then by fitting a sinusoidal curve to the data (Fig. 3). Distortion extent and orientation are then deduced by the maxima and minima of the sinusoidal curve, which correspond to the major and the minor ellipse axes, respectively. In particular, the ellipse orientation is given by the x-values of maxima and minima.

A similar procedure is carried out on the HRTEM images. In this case, the interplanar distances of the (1 0 0), (0 1 0), ($\bar{1}$ 0 0), (0 $\bar{1}$ 0) and (1 1 0), (1 $\bar{1}$ 0), ($\bar{1}$ 1 0), ($\bar{1}$ $\bar{1}$ 0) planes and the angles

that their normals form with the x-axis are measured (Table 2) and plotted (Fig. 4).

We remark here that the numerical values reported in Tables 1 and 2, as well as the related Figs. 3 and 4, are of course valid only for the present experiment and the microscope we used. With a different microscope, these values might be different in magnitude and orientation, or this distortion might even not exist at all.

3.2. Curve fitting

In order to calculate the main axes of the distortion ellipse, the nonlinear least-squares method was applied (Numeric recipes in C++ [22]). The model equation for the data sets can be expressed as

$$f(x) = off + A\sin(kx + b),$$

where off is a vertical offset of the sine wave, A and k are scale coefficients and b is a phase shift. The value of the k coefficient is 2, since there are two maxima on the data chart (Figs. 3 and 4).

The three variables may be obtained using Microsoft® Excel or any other software package for mathematical calculations. If one uses the Excel program, the add-in named "Solver" must be installed using the installation disk and activated during an Excel session, as the option is not installed by default. Table 3

Table 2
Orientations of the direct vectors with respect to the horizontal reference *x*-axis and normalized values (with respect to the average) of the interplanar distances, at different magnifications (images collected on image plates)

| Magnification	400k ×		600k ×		800k ×		1M ×	
	Angle (deg)	$d_{hkl}/\langle d_{hkl}\rangle$	Angle (deg)	$d_{hkl}/\langle d_{hkl}\rangle$	Angle (deg)	$d_{hkl}/\langle d_{hkl}\rangle$	Angle (deg)	$d_{hkl}/\langle d_{hkl}\rangle$
[1 1 0]	−50.7	0.9937	−51.0	0.9930	−50.3	0.9939	−50.6	0.9930
[1 0 0]	−5.1	0.9955	−5.3	0.9937	−4.5	0.9944	−4.8	0.9949
[1 −1 0]	39.9	1.0070	39.8	1.0074	40.3	1.0066	40.3	1.0064
[0 −1 0]	84.2	1.0037	84.1	1.0059	84.6	1.0050	84.5	1.0057
[−1 −1 0]	129.3	0.9937	129.0	0.9930	129.7	0.9939	129.4	0.9930
[−1 0 0]	174.9	0.9955	174.7	0.9937	175.5	0.9944	175.2	0.9949
[−1 1 0]	219.9	1.0070	219.8	1.0074	220.3	1.0066	220.3	1.0064
[0 1 0]	264.2	1.0037	264.1	1.0059	264.6	1.0050	264.5	1.0057

d_{h00} and d_{0h0} values divided by $2^{1/2}$.
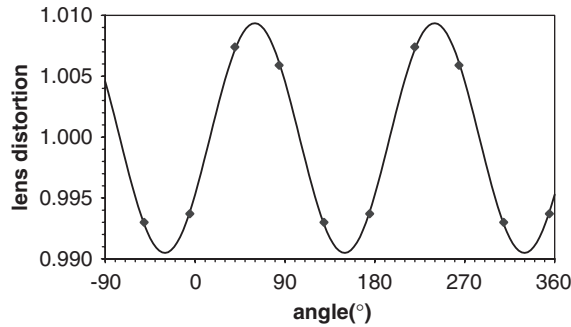
Fig. 4. Lens distortion in image mode, given as ratios between observed and average interplanar spacings ($d_{hkl}/\langle d_{110}\rangle$), versus orientation to the reference horizontal *x*-axis for 600k ×.

reports an example of input (data from Table 1, 200 cm).

The initial set of coefficients is in cells E2–E4. This set can be estimated from the initial data as follows:

(i) The offset *off* (cell E3) must be 1.0, since the ratio along any two non-parallel directions chosen on the image must be equal to 1.0 in the perfect case.
(ii) The scale factor *A* (cell E2) can be selected as the maximum value (cell C12 with equation = MAX(C2:C11)) of $|d_{hkl,\mathrm{norm}} - off|$ (cell range C2–C11).
(iii) The value of phase shift *b* (cell E4) can be initialized to 0.

The calculated values of the model function are in the F2–F11 cells. F2 contains equation

= E2*SIN(2*RADIANS(*A*2) + E4) + E3

which is applied to the whole range of cells. As Excel accepts all arguments for trigonometric functions in radians, degrees must be converted into radians.

The cell G2 contains the equation = F2−B2 which is the difference between the experimental (cell B2) and calculated data (cell F2). The sum of squared differences is in the cell H2 with the equation = SUMSQ(G2:G11). The Solver add-in minimizes this sum by varying cells (E2–E4). Fig. 5 shows the Solver dialog box, with all the fields needed to find the optimal solution filled in. Results are presented in Table 4.

The minimum/maximum of the model function closest to the zero point can be found by solving the first-order differential equation d/d*x* *f*(*x*) = 0. The formal solution can be expressed as $2x + b = (\pi/2) + \pi n$. Then, the value of *x* in the first quadrant can be calculated with *n* = 0:

$$x = \frac{\pi}{4} - \frac{b}{2},$$

obtaining the main direction of the distortion ellipse, in the present case equal to 63.43°. This angle is calculated by equation (cell E7)

= D*EGREES*(PI()/4-E4/2),

Table 3
Excel example of initial data set before parameters estimate

	A	B	C	D	E	F	G	H
1	Angle	$g_{hkl}/\langle g_{hkl}\rangle$	$|d_{hkl}-off|$			y(calc)	Delta	Sum_sq
2	−57.8	0.995485	0.00452	a	0.00834	0.992476	−0.003009	0.000166
3	−12.2	0.991670	0.00833	offset	1	0.996566	0.004896	
4	33.3	1.004509	0.00451	b	0	1.007657	0.003148	
5	77.6	1.008336	0.00834			1.003489	−0.004848	
6	122.2	0.995485	0.00452			0.992476	−0.003009	
7	167.8	0.991670	0.00833	b(deg)	0	0.996566	0.004896	
8	213.3	1.004509	0.00451	distort	1.0168	1.007657	0.003148	
9	257.6	1.008336	0.00834			1.003489	−0.004848	
10	302.2	0.995485	0.00452			0.992476	−0.003009	
11	347.8	0.991670	0.00833			0.996566	0.004896	
12		Max =	0.00834					

Table 4
Excel example showing the optimal solution

|	A	B	C	D	E	F	G	H
1	Angle	$g_{hkl}/\langle g_{hkl}\rangle$	$|d_{hkl}-off|$			y(calc)	Delta	Sum_sq
2	−57.8	0.995485	0.00452	a	0.009462	0.995538	5.28E-05	5.41E-08
3	−12.2	0.991670	0.00833	offset	0.999912	0.991615	−5.5E-05	
4	33.3	1.004509	0.00451	b	−0.64342	1.004606	9.66E-05	
5	77.6	1.008336	0.00834			1.008241	−9.5E-05	
6	122.2	0.995485	0.00452			0.995538	5.28E-05	
7	167.8	0.991670	0.00833	b(deg)	63.4325	0.991615	−5.5E-05	
8	213.3	1.004509	0.00451	distort	1.01911	1.004606	9.66E-05	
9	257.6	1.008336	0.00834			1.008241	−9.5E-05	
10	302.2	0.995485	0.00452			0.995538	5.28E-05	
11	347.8	0.991670	0.00833			0.991615	−5.5E-05	
12		Max =	0.00834					
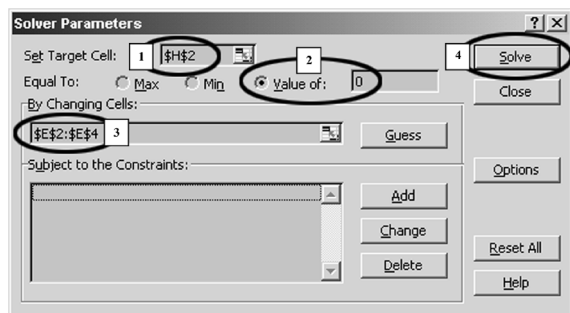
Fig. 5. Solver dialog box from the Microsoft® Excel program. The target cell (1) should be minimized (its value should be as close to zero as possible (2)) by changing cells (3). The Solve button (4) must be pressed to proceed with minimization.

and corresponds to the position of the first maximum in the range of angles between $-\pi/2$ and $\pi/2$ (see Figs. 3 and 4).

The value of the maximal distortion is calculated as a scale factor along the major axis of the distortion ellipse by the equation (in the cell E8)

$$= (1 + E2)/(1 - E2).$$

The results of calculations over all our data are presented in Tables 5 and 6. Depending on the camera length, the maximal distortion in diffraction mode occured at 60.5–63.5°, with values increasing with magnification from 1.6% to 1.9%. In the HRTEM mode, the maximal

Table 5
Results of fitting for different camera lengths

Camera length (cm)	Distortion direction (deg)	Maximal distortion
200	63.43	1.0191
150	63.18	1.0173
120	60.50	1.0156

Table 6
Results of fitting for different magnifications

Magnification (k ×)	Distortion direction (deg)	Maximal distortion
400	55.81	1.0157
600	59.71	1.0190
800	60.26	1.0167
1000	58.98	1.0174

distortion occurred between $55.8°$ and $60.3°$, depending on magnification. If the crystal were oriented such that the distortion is exactly along one of the crystal axes, then the lengths of the 100 and 010 vectors would be different, while the angle between them remains exactly $90°$. For this orientation, the diagonals 110 and $1\bar{1}0$ would be measured as equally long, but they would not be at $90°$ to each other. A distortion of 1% (i.e. making a circle into an ellipse with main axes lengths 0.99 and 1.01) would result in a maximal error of a right angle going from $90.0°$ to $91.1°$. This can be seen from the data in Table 1: the maximal elongation is nearly along the $\bar{1}10$ direction, which is 1.5% longer than the 1 1 0, the two directions being nearly at right angles, $89.7°$ apart. On the other hand, 200 and 020 differ by only 0.4% in length, but the angle between them is significantly off from $90°$; it is $89.1°$.

In order to check if the distortion came from the electron microscope or from the imaging plate scanning, we also recorded SAED patterns on photographic film and measured the same distances between diffraction points as above. Such a measurement can be done with accuracy to within 0.1%, even using a ruler and a light-box. The results were identical to the ones obtained with the

imaging plates, proving that the distortion came from the electron microscope. We have also performed the same analysis on TEMs at Stockholm University and found quite similar results, although the exact angle and magnitude of elongation were of course not the same.

3.3. Compensating for the distortions

Finally, once the distortions have been quantitatively determined, they should be compensated for. We did this in the following way. Each image is first rotated in order to bring the distortion axis of maximal elongation on the horizontal x-axis. Then the image or ED pattern is stretched along the vertical direction by the calculated maximal distortion value (or compressed by the same value along the horizontal direction). Finally, the scale factor for the stretched image must be multiplied by the amplitude of maximal distortion before performing further calculations with the image.

4. Discussion and conclusions

The closeness of the distortion directions within a single imaging mode for different magnifications and between the two different modes indicates that the imperfection lies in the projector lens, which is used in both HRTEM and SAED modes.

The method described is very effective in detecting lens distortion. Moreover, it provides a way to correct it. Although in the present case it has been applied on data acquired with imaging plates and conventional photographic films, in principle it can be applied with any type of acquisition device, including CCD cameras, and even operate online, if the appropriate equipment is available.

The amended data can also be used to calibrate the actual magnification and camera length values of the microscope, provided that highly accurate cell constants are known from other experiments (Table 7). In our case, by refinement of X-ray powder diffraction data from the same compound, we obtained $a = 15.6388(3)$ and $c = 13.0915(3)$,

Table 7

Actual camera constants and magnifications (column 4) after calibration using accurately known unit cell dimensions ($d_{110} = 11.058$ Å), as compared with the nominal values (column 2)

L, Mag	$L\lambda$, k $\times$	d_{110} (Å)	$L\lambda$, k $\times$
120 cm	30.12	10.883	30.60
150 cm	37.65	10.858	38.34
200 cm	50.20	11.334	48.98
400k $\times$	400	10.166	367.73
600k $\times$	600	10.144	550.41
800k $\times$	800	10.169	735.68
1M $\times$	1000	10.375	938.23

Table 8

Rotation (deg) between diffraction patterns and images at different camera lengths and magnifications

L	400k $\times$	600k $\times$	800k $\times$	1M $\times$
120 cm	29.1	29.3	28.5	28.8
150 cm	31.2	31.4	30.6	30.9
200 cm	38.4	38.6	37.8	39.1

with a d_{110} distance of 11.058 Å. The latter value was used to calculate the actual camera constants[1] and magnifications (column 4). We found deviations from the nominal values as high as $\approx 2.5\%$ for camera constants and $\approx 8.3\%$ for magnifications. It should be noted, however, that better accuracy in deriving absolute values can be obtained, whenever possible, if one uses a dispersed standard and measures the cell constants of the specimen under investigation and those of the standard on the same exposure.

Finally, the reciprocal rotations in the microscope column between the images and the related diffraction patterns at different magnification/camera lengths can be deduced (Table 8).

Of course, the present results strictly refer to our experiments only, in the given microscope. As totally different values of distortion orientation

and distortion extent may occur elsewhere, we recommend that similar checks be made also in other laboratories, working with different equipment or using different alignment procedures.

Notwithstanding the possible interlaboratory variability, we feel that our results may have a major, general importance. In fact, most often electron diffraction is considered as just a qualitative tool only, being affected by many aberrations connected to the magnetic lenses. Therefore, in many cases authors do not even attempt to exploit the observed lattice parameters. At present, this choice may be quite limiting, because of the current evolution towards nanosciences that demand definitely quantitative data. Namely, it would be nice to be able to easily determine realistic lattice parameters using electron diffraction or lattice images only. Our procedure may perhaps help to ameliorate the current accuracy of lattice parameter determinations. The smaller the size of nanoscience problems, the greater the need of simple, quantitative exploitation of HRTEM images and diffraction patterns.

An extreme field where this kind of correction may be mandatory is the study of strained lattice cell parameters in nanophases [23], to ascertain whether the observed strain effects are real, and what is their precise extent.

Similarly, another field where this approach may be very important is symmetry determination. In several cases, scientists doing HRTEM observations suggest that the actual symmetry was lower than that found by X-ray diffraction. Supporting evidence was given by unmatching symmetry-related parameters, or by angles in TEM images slightly deviating from 90° [24,25]. Here too, we feel that before drawing any major conclusion, images should first be corrected for any possible bias, such as the elliptical distortion described here.

A final issue regards the long-term reproducibility of the correction factors, namely whether they are a constant of a given microscope, or may change over time, due to short-term effects like lens hysteresis or long-term effects connected with major alignment or maintenance procedures. Here, we suggest frequent checks of the elliptical distortion of images and SAED patterns, in order

---

[1]The camera constant ($L\lambda$) can be calculated from the relation $d_{hkl} = L\lambda/R$, where d_{hkl} is the interplanar distance (11.058 Å in our case), L is the camera length in mm, λ is the electron wavelength in Å (0.0251 for 200 kV) and R is the measured reciprocal lattice distance in mm of the hkl reflection.

to determine if and how the distortions vary with time.

Acknowledgments

References

[1] P.N.T. Unvin, R. Henderson, J. Mol. Biol. 94 (1975) 425.

[2] R. Henderson, J.M. Baldwin, T.A. Ceska, F. Zemlin, E. Beckmann, K.H. Downing, J. Mol. Biol. 213 (1990) 899.

[3] W. Kühlbrandt, D.N. Wang, Y. Fujiyoshi, Nature 367 (1994) 614.

[4] D.L. Dorset, W.F. Tivol, J.N. Turner, Ultramicroscopy 38 (1991) 41.

[5] W. Dong, T. Baird, J.R. Fryer, C.J. Gilmore, D.D. MacNicol, G. Bricogne, D.J. Smith, M.A. O'Keefe, S. Hovmöller, Nature 355 (1992) 605.

[6] I.G. Voigt-Martin, D.H. Yan, C.J. Gilmore, K. Shankland, G. Bricogne, Ultramicroscopy 56 (1994) 271.

[7] S. Hovmöller, A. Sjögren, G. Farrants, M. Sundberg, B.O. Marinder, Nature 311 (1984) 238.

[8] T.E. Weirich, R. Ramlau, A. Simon, S. Hovmöller, X. Zou, Nature 382 (1996) 144.

[9] X. Zou, S. Hovmöller, M. Parras, J.M. Gonzáles-Calbet, M. Vallet-Regí, J.C. Grenier, Acta Crystallogr. A 49 (1993) 27.

[10] Y.D. Mo, T.Z. Cheng, H.F. Fan, J.Q. Li, B.D. Sha, C.D. Zheng, F.H. Li, Z.X. Zhao, Supercond. Sci. Technol. 5 (1992) 69.

[11] Z.Q. Fu, H.F. Fan, Ultramicroscopy 54 (1994) 229.

[12] S. Hovmöller, Ultramicroscopy 41 (1992) 121.

[13] Z.H. Wan, Y.D. Liu, Z.G. Fu, Y. Li, T.Z. Cheng, F.H. Li, H.F. Fan, VEC—Visual Electron Crystallography, Institute of Physics, Chinese Academy of Sciences, Beijing 100080, China, 1992–2000.

[14] X. Zou, Y. Sukharev, S. Hovmöller, Ultramicroscopy 49 (1993) 147.

[15] C.J. Gilmore, G. Bricogne, in: C.W. Carter Jr, R.M. Sweet (Eds.), Methods in Enzymology, vol.277, Academy Press, New York, 1997, p. 65.

[16] M. Gemmi, Ph.D. Thesis, Bologna University, Italy, 1999.

[17] P. Hirsch, A. Howie, R. Nicholson, D.W. Pashley, M.J. Whelan (Eds.), Electron Microscopy of Thin Crystals, Krieger Publishing Company, Malabar, Florida, 1977.

[18] K. Tsuno, Y. Harada, J. Phys. Eng.: Sci. Instrum. 15 (1981) 313.

[19] K. Tsuno, Y. Harada, J. Phys. Eng.: Sci. Instrum. 15 (1981) 955.

[20] K. Tsuda, M. Tanaka, Acta Crystallogr. A 55 (1999) 939.

[21] D.J. Smith, W.O. Saxon, M.A. O'Keefe, G.J. Wood, W.M. Stobbs, Ultramicroscopy 11 (1983) 263.

[22] W.H. Press, W.T. Vetterling, S.A. Teukolsky, B.P. Flannery, Numerical Recipes in C++, second ed., Cambridge University Press, Cambridge, 2002.

[23] C. Ferraris, L. Folco, M. Mellini, Phys. Chem. Miner. 30 (2003) 503.

[24] I. Dódony, M. Posfài, P.R. Buseck, Am. Mineral. 87 (2002) 1443.

[25] H.H. Hng, K.M. Knowles, P.A. Midgley, J. Am. Ceram. Soc. 84 (2001) 435.